An Intercomparison of the Dynamical Cores of Global Atmospheric Circulation Models for Mars

A NASA Ames Research Center Joint Research Interchange
Final Report

Jeffery L. Hollingsworth*†, Alison F. C. Bridger♭ & Robert M. Haberle†

University Consortium Agreement: NCC2-5171
Project Duration: 26 February 1996–25 February 1998

*San Jose State University Foundation, P.O. Box 720130, San Jose, California 95172, USA
†NASA Ames Research Center, MS: 245-3, Moffett Field, California 94035, USA
♭Department of Meteorology, San Jose State University, San Jose, California 95192, USA

ABSTRACT

This is a Final Report for a Joint Research Interchange (JRI) between NASA Ames Research Center and San Jose State University, Department of Meteorology. The focus of this JRI has been to evaluate the dynamical "cores" of two global atmospheric circulation models for Mars that are in operation at the NASA Ames Research Center. The two global circulation models in use are fundamentally different: one uses spherical harmonics in its horizontal representation of field variables; the other uses finite differences on a uniform longitude-latitude grid. Several simulations have been conducted to assess how the dynamical processors of each of these circulation models perform using identical "simple physics" parameterizations. A variety of climate statistics (e.g., time-mean flows and eddy fields) have been compared for realistic solstitial mean basic states. Results of this research have demonstrated that the two Mars circulation models with completely different spatial representations and discretizations produce rather similar circulation statistics for first-order meteorological fields, suggestive of a tendency for convergence of numerical solutions. Second and higher-order fields can, however, vary significantly between the two models.

1. INTRODUCTION

A valuable method for moving systematically toward improved models of climate—in particular, to identify internal and external agents most sensitive to, and responsible for, climate change—is the careful evaluation and intercomparison of standardized simulations from independently constructed atmospheric global circulation models (AGCMs) [*Gates*, 1992]. To attribute differences among simulations to specific model properties, the intercomparison need to be cast accurately against a common framework. In this approach, the strengths and weaknesses of individual models may be unambiguously assessed. This holds for simplified and complex climate models not only of Earth but of Mars, as well.

AGCMs are based on the equations of motion for the time evolution of the full 3D flow field and of the thermodynamic state of the atmosphere. In the most sophisticated AGCMs, the set of equations, referred to as the meteorological primitive equations (PE) [*Holton*, 1992], includes detailed complex

physics for "right hand side" terms in the system (e.g., radiative-transfer physics yielding explicit diabatic heating rates). These types of global models are thus computationally very intensive. Simple physics primitive equations (SPPE) are AGCMs with simplified forms for the physics that drive the circulation, yet they do not compromise the dynamical formulation of the 3D flow. SPPE models are efficient "mechanistic" tools which can be used to examine particular components of the atmospheric circulation (e.g., the zonally symmetric circulation, the transient circulation, the stationary circulation, etc.) and their interactions. And since computations related to the driving physics are minimized, SPPE models are effective numerical tools for performing very long simulations aimed at addressing questions related to internal long-term climate variability.

While evaluation of full AGCMs is essential, the number of choices regarding physical parameterizations and sub-grid scale processes is large, so that it remains a challenge to comprehensively contrast even closely related models [*Gates*, 1992; *Held and Suarez*, 1994]. Every AGCM solves discrete forms of the governing equations. Careful examination of standard numerical methods used to discretize these equations is necessary to ascertain the degree of solution stability, accuracy and simulation convergence. For climate models, it is fundamentally important to assess directly the long-term statistics imposed by the dynamical-core "processor" (i.e., those intrinsic to the particular numerical and discretization methods used in the AGCM), which can influence the accuracy of short-term, deterministic solutions [*Held and Suarez*, 1994].

At the NASA Ames Research Center, two Mars AGCMs exist: a full, complex physics Mars general circulation model (MGCM) [*Pollack et al.*, 1981; *Pollack et al.*, 1990; *Haberle et al.*, 1993; *Haberle et al.*, 1997b;]; and a SPPE Mars climate model (MCM) [*Haberle et al.*, 1997a; *Houben et al.*, 1997]. The computationally intensive MGCM is used to determine detailed circulation statistics using the best implementation of *all* physical processes known to drive Mars' circulation. The more efficient mechanistic MCM is used to examine particular components of the circulation, to understand parameter sensitivity studies (e.g., determining the response to thermal relaxation and momentum dissipation strengths), and to carry out multi-annual simulations of internally or externally driven variability of Mars climate.

Under the primary task of this research proposal, the degree of convergence of the two Mars AGCMs in use at Ames has been investigated. In particular, the isolation and intercomparison of the dynamical-core processors intrinsic to each model has never been documented. Prior to presenting the key results of this investigation, a brief summary of the formulations of the two Mars AGCMs is outlined below.

1. The Ames Mars General Circulation Model (MGCM)

The NASA Ames MGCM is a finite-difference, complex physics Mars AGCM. Dependent variables in the MGCM are staggered in the horizontal and vertical directions, and the particular differencing scheme conserves energy and mean square enstrophy. The model uses a terrain-hugging vertical coordinate, whereby spatially varying topography at the model's surface can be handled correctly. Nominal resolution of the MGCM is 7.5° latitude × 9.0° longitude, with with 16–26 vertical levels extending up to approximately 60–100 km.

The MGCM's heating routines allow for a diurnal cycle, a surface heat budget, radiative effects of CO_2 gas and suspended aerosols (e.g., dust and/or water condensates), latent heat release associated with CO_2 condensation, and heat exchange between the atmosphere and surface. Surface friction is parameterized using a bulk boundary-layer scheme. Near the model top, a Rayleigh friction "sponge layer" is applied to help dissipate upward propagating waves and spurious downward reflection of wave energy. To save computational time, radiative fluxes are computed using look-up tables created off line

using a CO_2 line-by-line code and a multi-spectral doubling code for dust. Further documentation on the nature of Mars' climate as simulated by the MGCM and details of the MGCM's physical processes are provided in *Pollack et al.* [1990]; *Haberle et al.* [1993]; and *Haberle et al.* [1997b].

2. The Ames Mars Climate Model (MCM)

The NASA Ames Mars MCM is spectral, simple physics Mars AGCM. This SPPE model was adapted from that of *Young and Villere* [1985] to investigate aspects of Mars' 3D atmospheric circulation and the nature of its climate. For computations of the dependent variables, the MCM uses a spectral (spherical harmonic) representation in the horizontal and finite differences in the vertical. Typical truncations that have been used are 16Tr06L14 (corresponding roughly to a 5.5° latitude × 18° longitude nonuniformly spaced "physical" grid, with 14 vertical levels extending up to approximately 47 km), and 30Tr10L16 (roughly 3.7° latitude × 11.3° longitude, with 16 vertical levels extending up to approximately 56 km). In the vertical, the layer spacing is unequal in log-pressure height, $z \equiv -H \ln(p/p_s)$. The MCM uses simple physical parameterizations: diabatic heating is specified in terms of a meridionally dependent thermal relaxation (Newtonian cooling) towards a "radiative equilibrium" temperature field, and momentum drag is specified in terms of a height-dependent drag (Rayleigh friction). The prescribed zonally symmetric radiative equilibrium thermal field as a function of latitude, height and season is independently determined using results from a 1-D radiative-convective model [*Haberle et al.*, 1997b]. A parameterization for the seasonal condensation of CO_2 onto the polar caps is also included.

The MCM has been used successfully to investigate the zonally symmetric (Hadley) circulation and its interactions with transient circulation components (i.e., eddies associated with barotropic and/or baroclinic processes) [*Haberle et al.*, 1997b]. And, the MCM has been used in full 3D simulations of the seasonal cycle of Mars' water cycle which incorporates a parameterization of regolith adsorption [*Houben et al.*, 1997].

2. KEY RESULTS OF INVESTIGATION

By performing a series of carefully designed fixed-season simulations, the primary objective of this research proposal has been to systematically evaluate the dynamical processors of th two Mars global circulation models in operation at NASA Ames. This evaluation has revealed key aspects of each processor unmasked from complex physical parameterizations used in the different models. A secondary objective of this proposal has been to initiate the movement toward the creation of modular Mars climate dynamical processors which could become "plug-compatible" with different physical parameterizations modules that can be easily interchanged.

The radiative heating-cooling algorithms in the MGCM were extracted, and algorithms for simplified forcings in terms of spatially dependent thermal (Newtonian) relaxation rates and radiative equilibrium fields for a specified season were inserted. In this approach, the prognostic equation for atmospheric temperature has the simple form $\partial T/\partial t \propto -\alpha_N(\varphi,\sigma)(T - \overline{T}_{eq}(\varphi,\sigma;L_s))$, where $\sigma \equiv (p - p_{trop})/(p_s - p_{trop})$ is the MGCM's vertical coordinate. In addition, algorithms related to boundary-layer processes were extracted and a subroutine for a height dependent momentum dissipation (Rayleigh drag) was inserted. This required an additional term in the prognostic equations for horizontal momentum, namely $\partial \mathbf{v}/\partial t \propto -\alpha_R(\varphi,\sigma)\mathbf{v}$, where $\mathbf{v} = (u,v)$ is the horizontal wind vector.

In the dynamical-core checks, the MGCM used a "flat" lower boundary condition (i.e., no surface topography, thermal inertia and albedo). In addition, both models used the same vertical domain (L16), with a tropopause pressure, $p_{trop} = 10^{-3}$ mbar (roughly 60 km). However, horizontal resolutions differed between the two models; the MGCM used 7.5° latitude × 9.0° longitude and the MCM used a and 30Tr10L16 truncation (roughly 3.7° latitude × 11.3° longitude).

a. Comparisons of Time and Zonally Averaged Mean States

Using the dynamical-core version of the MGCM, several 50-day simulations have been performed for northern winter conditions without atmospheric dust loading using a moderate radiative-relaxation time constant (i.e., $L_s = 270°$, $\tau = 0$, $\tau_{radeq} = 2$ days). The prescribed radiative-equilibrium temperature field is identical to that presented in Figure 1a of *Haberle et al.* [1997b]. Shown in Figure 1 are latitude-pressure cross sections of the time and zonally averaged zonal wind and temperature fields, as well as the mean mass stream function from one simulation. Time averages were computed over the last 30 days of simulation.

A substantial meridional temperature gradient exists in middle and high latitudes of the winter hemisphere. In the presence of such strong temperature gradients and by thermal wind balance, a significant westerly jet develops in the extratropics (Figure 1a) which extend deeply in the vertical through 6 scale heights. The westerly jet core, $O(150\ \mathrm{m\ s^{-1}})$, is located just on the poleward side of the warm protrusion in midlatitudes. The latter results from compressional heating occurring within the descending branches of the Hadley circulation cells (Figure 1b) which emanates from low levels near the sub-solar point. The magnitude of the seasonal mean and longitudinally averaged meridional circulation is moderate: meridional and vertical winds are between (+/-) $O(15–25\ \mathrm{m\ s^{-1}})$ and $O(5–10\ \mathrm{cm\ s^{-1}})$, respectively, with extrema near the 0.03–0.1 mbar level. The reverse circulation in high northern latitudes, the "Ferrel cell", is a result of transient eddies, traveling from west-to-east around the planet. Such time and zonally averaged mean fields are in fact very similar to those produced by the spectral MCM (presented in Figures 3 and 4 of *Haberle et al.* [1997b]), indicating very similar equilibrated mean circulations have been reached even though the two models have very different (discrete) representations of atmospheric field variables and rather different horizontal resolutions.

For different seasons (e.g., equinox) and dust loadings, time and zonally averaged atmospheric fields are also rather similar between the dynamical-core version of the MGCM and the spectral MCM.

b. Comparisons of Transient Eddy Statistics

When comparisons are made between second- and higher-order field variables, differences between the two models become apparent. Shown in Figure 2 are latitude-pressure cross sections of various transient eddy statistics. These fields have been obtained by band-pass filtering temporal deviations from time mean fields so as to isolate circulation variability on the synoptic time scale (i.e., periods of $O(2–8$ days)). The eddy kinetic energy (Figure 2a) shows quite large transient activity in the northern extratropics that increases with altitude within the westerly waveguide. Eddy geopotential height (Figure 2b) shows a similar distribution in midlatitudes where the amplitude increases with increasing height; however substantial activity is also apparent at high altitude in the subtropics. The transient covariance of meridional wind and temperature shows (Figure 2c) quite large poleward heat flux in the subtropics at low levels that tilts poleward in mid- and high-latitudes, and decreases rather rapidly with height (e.g., over 3–5 scale heights). This spatial pattern is consistent with the vertical propagation of transient eddy activity from low levels within the westerly jet. It is also indicative of the conversion of zonal to eddy available potential energy in the life cycle of the transient disturbances.

In the spectral model, the transient eddies show some similarities with those seen in the dynamical-core version of the MGCM yet there are also distinct differences, particularly in the spatial distribution of eddy variances and covariances. Transient statistics diagnosed from and identical MCM simulation are shown in Figure 3 (the same contour intervals are used for comparisons). It can be seen that the eddy kinetic energy is much larger in the extratropics (Figure 3a) and shows a secondary maximum $O(300\ \mathrm{m^2\ s^{-2}})$ in the subtropics at mid- to upper-levels not seen in the MGCM. The eddy geopotential height spatial pattern (Figure 3b) is similar in its spatial distribution; however, the peak magnitude at

upper levels in the extratropics is larger by nearly a factor of two. Overall, the transient eddies in the MCM appear much more vigorous where, for example, they transport more heat poleward and through a deeper vertical column in the winter extratropics (Figure 3c) by factors of 3–5. Furthermore, comparing the transient meridional momentum transports (not shown), the eddies in the MCM also appear more barotropic in nature. In particular, there is considerable equatorward transport (4–5 times greater) on the equatorward side of the jet at mid- to upper-levels in the MCM, indicative of westerly momentum transport into the easterly summer jet, and considerable barotropic production of kinetic energy. Momentum transports in the winter extratropics at low- to mid-levels do appear similar between the MCM and MGCM, however.

c. Large-Scale Topography Sensitivity Experiments

The dynamical-core version of the MGCM has also been used to mechanistically examine some effects played by Mars' large-scale topography on the winter circulation. In particular, interactions between the zonally symmetric circulation, the topographically forced stationary circulation and the transient components have been explored. The model's surface topography is taken from the dataset deduced by Smith and Zuber (1996) which is derived using an eighth-degree and order spherical harmonic model with half-wavelength resolution of 1350 km, and reanalyses of Mariner 9 and Viking Orbiter occultation data.

In Figure 4 are shown latitude-pressure cross sections of transient fields but for an experiment that included surface topography. The spatial patterns of eddy kinetic energy and geopotential height appear rather similar; however in the no topography experiment, the vertical gradients and the peak values at high altitude are are much stronger. The effectiveness of the transient eddies to transport heat poleward is reduced tremendously when topography is included (Figure 4c): below 1–2 scale heights the heat transports are weaker by a factor of seven or more. In the presence of significant pole-to-equatorward temperature contrasts, the stationary component of the circulation as can be seen in Figure 5, contributes substantially to the poleward transports of heat and momentum particularly in the extratropics. Stationary eddy kinetic energy and geopotential height are quite comparable to the transient contributions (cf. Figure 4). There is significant stationary amplitudes at low-levels in the summer extratropics that is associated with the shallow westerly waveguide in this hemisphere, which decay rapidly above 1-2 scale heights from the surface forcing. However, the stationary heat transports exceed the transient contributions in middle and high latitudes, and they occur over a deeper region.

From a few other mechanistic simulations with the MGCM, it appears that competition and interference between a large-amplitude stationary component in middle latitudes and the synoptic transient components can be quite significant. In the presence of large asymmetric topographic forcing, not only does the stationary circulation become a key player in heat and momentum transport toward the winter hemisphere, there also is a change in the dominant spatial scales of the transient disturbances as can be seen in Figure 6). In the no topography experiments, the meridional wind variance near the 3.0 mbar level peaks at wavenumber 3 in midlatitudes. There is also a pronounced wavenumber 1 component at very high latitudes. The meridional heat flux zonal spectra, shows a similar peak at wavenumber 3. However, when topography is included not only are the amplitudes of the disturbances much weaker, the zonal scale of the transient disturbances shifts to longer wavelengths (i.e., zonal wavenumber 2 predominantly). There is also an apparent "splitting" near 40° of the predominant zonal scale of the disturbances in middle and high latitudes, and those in the subtropics, the latter of much shorter wavelength (i.e., zonal wavenumber 4).

Furthermore, experiments with scaled versions of the large-scale topography show that with decreasing amplitude of orographic forcing, the transient variability shifts toward lower frequency (i.e.,

longer period modes), maximizes roughly 10 deg equatorward, and appears more barotropic in structure. This occurs despite the fact the mean baroclinicity remains rather similar throughout the range of scaled topographic experiments. Shown in Figure 7) are the stationary components for an experiment in which the topography field has been scaled by 0.2. The stationary eddy kinetic energy is much reduced in this case. However, it can be seen that the westerly waveguide is intrinsically sensitive to even weak stationary forcing, where peak stationary eddy geopotential heights are nearly comparable to the full-topography values (cf. Figure 5). Yet, because the vertical gradients (i.e., stationary eddy temperatures) are much weaker, there is only a weak effective poleward heat transport by the stationary component of the circulation in this simulation.

From a series of simulations performed with the dynamical-core GCM, surface pressure time series have been analyzed using singular spectrum analysis (SSA) and autoregressive models (cf. Penland et al., 1991) to estimate the power spectra associated with circulation variability in the simulations. Comparisons have also been made with the Viking Lander 2 pressure data. Using the SSA adaptive-filtering technique, it has been found that the GCM exhibits synoptic periods in rather good agreement with the observations (Barnes, 1980). Shown in Figure 8 are surface pressure time series for the MGCM grid point nearest the Viking Lander 2 location for the no-topography, full-topography and scaled-topography experiments. It can be seen that the dominant O(2–4 days) period in the no-topography and scaled-topography cases are similar. However with full topography, there are two dominant modes: a long-period mode of O(6–8 days) that modulates the shorter period modes of O(2–4 days).

3. DISCUSSION AND AREAS FOR FUTURE WORK

Understanding the dynamical-core processors of two AGCMs for Mars' atmosphere in operation at the NASA Ames Research Center has been the primary focus of research under this agreement. This has included analyses of transient eddy activity for nearly identical experiments with the two models and sensitivity studies of the forced and transient circulations to prescribed mechanistic external forcing (e.g., surface topography) with the core version of the MGCM. We have, nevertheless, only analyzed a small subset of mechanistic simulations and it would be prudent to continue efforts on this topic as it relates to convergence of the numerical solutions as a function of assumed horizontal and vertical resolutions, as well convergence as a function of assumed radiative-equilibrium thermal relaxation fields and prescribed dissipations. Further more detailed analyses of globally integrated mean-zonal available potential and kinetic energy, eddy available and kinetic energy, and barotropic-baroclinic energy conversions should be included in such simulations. To this end, careful decomposition could be applied in terms of a transformed Eulerian mean (TEM) formulation of the atmospheric energy cycle [*Plumb*, 1983]. This alternative formulation of the energetics has the advantage in that there is a single conversion from eddy-to-mean components, in contrast to a separation between baroclinic and barotropic processes [*Grotjahn*, 1993; *James*, 1994].

In addition, regarding the separation of temporal and spatial scales, the spatial structure and variability in the dynamical-core simulations could be assessed using the method of empirical orthogonal function (EOF) analysis. This analysis scheme provides an extremely efficient way of describing geophysical time series in both space and time [*Peixoto and Oort*, 1992]. A covariance eigenvector/eigenvalue problem is generated from "observational" points within the numerical simulations, where the eigenvectors (i.e., EOFs) correspond to the intrinsic spatial structure of the variability of the original field variables, and the eigenvalues (i.e., principal components) are newly generated time series which explain a known percentage of the variability associated with each EOF [*Horel*, 1981; *Mo and Ghil*, 1987].

REFERENCES

Barnes, J. R., 1980: Time spectral analysis of midlatitude disturbances in the Martian atmosphere. *J. Atmos. Sci.*, **37,** 2002–2015

Gates, W. L., 1992: AMIP: The atmospheric model intercomparison project. *Bull. Amer. Meteor. Soc.*, **73,** 1962–1970

Grotjahn, R., 1993: *Global Atmospheric Circulations: Observations and Theories*, Oxford University Press, 430 pp.

Haberle, R. M., J. B. Pollack, J. R. Barnes, R. W. Zurek, C. B. Leovy, J. R. Murphy, H. Lee, and J. Schaeffer, 1993: Mars atmospheric dynamics as simulated by the NASA-Ames general circulation model I. The zonal-mean circulation. *J. Geophys. Res.*, **98,** 3093–3124

Haberle, R. M., H. Houben, J. R. Barnes, and R. E. Young, 1997a: A simplified three-dimensional model for Martian climate studies. *J. Geophys. Res.*, **102,** 9051–9067.

Haberle, R. M., J. R. Barnes, J. R. Murphy, Manoj M. Joshi, and J. Schaeffer, 1997b: Meteorological predictions for the Mars Pathfinder lander. *J. Geophys. Res.*, **102,** 13301–13311.

Held, I. M., and M. J. Suarez, 1994: A proposal for the intercomparison of the dynamical cores of atmospheric general circulation models. *Bull. Amer. Meteor. Soc.*, **75,** 1825–1830

Holton, J. R. 1992: *An Introduction to Dynamic Meteorology*, Academic Press, 511 pp.

Houben, H. C., R. M. Haberle, R. E. Young, and A. P. Zent, 1997: Modeling the Martian seasonal water cycle. *J. Geophys. Res.*, **102,** 9069–9083.

Horel, J. D., 1981: A rotated principal component analysis of the interannual variability of the northern hemisphere 500 mb height field. *Mon. Wea. Rev.*, **109,** 2080–2092

James, I. N., 1994: *Introduction to Circulating Atmospheres*, Cambridge University Press, 422 pp.

Mo, K. C., and M. Ghil, 1987: Statistics and dynamics of persistent anomalies. *J. Atmos. Sci.*, **44,** 877–901

Peixoto, J. P., and A. H. Oort, 1992: *Physics of Climate*, American Institute of Physics, 520 pp.

Plumb, R. A., 1983: A new look at the energy cycle. *J. Atmos. Sci.*, **40,** 1669–1688

Pollack, J. B., R. M. Haberle, J. Schaeffer, and H. Lee, 1990: Simulations of the general circulation of the Martian atmosphere I: Polar processes. *J. Geophys. Res.*, **95,** 1447–1473

Young, R. E. and G. L. Villere, 1985: Nonlinear forcing of planetary scale waves by amplifying unstable baroclinic eddies generated in the troposphere. *J. Atmos. Sci.*, **42,** 1991–2006

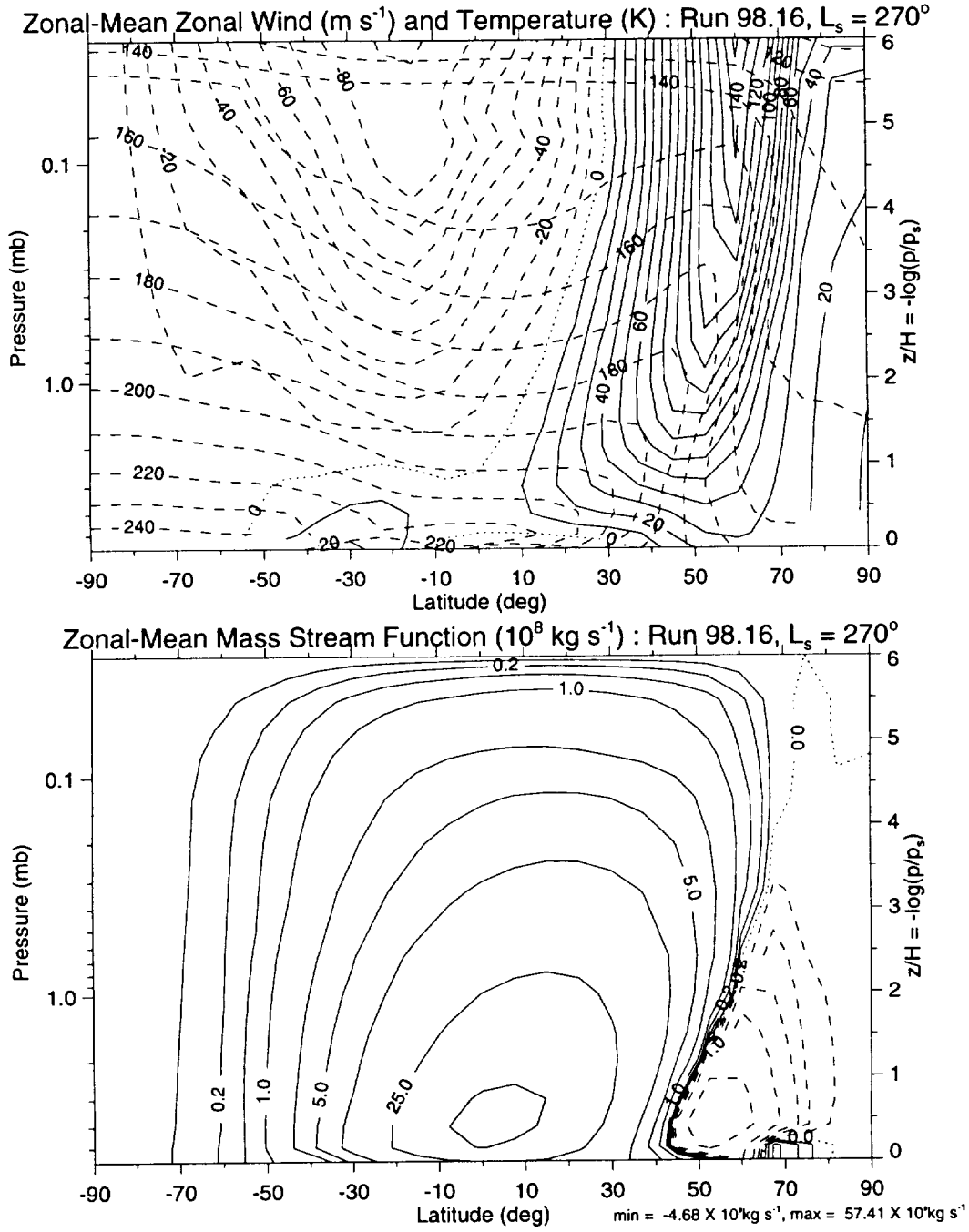

Figure 1: A dynamical core simulation with the Mars General Circulation Model (MGCM) at 7.5 × 9.0° horizontal resolution and 16 vertical layers (with no surface topography) using the $L_s = 270°$, $\tau = 0$ radiative-equilibrium relaxation field with a relaxation time constant $\tau_{radeq} = 2$ days: time and zonally averaged (a) zonal wind (m s^{-1}) and temperature (K), and (b) mass stream function ($\times 10^8$ kg s^{-1}). In (a), the solid (dashed) contours correspond to eastward (westward) wind and the dotted contour is the zero isopleth. The contour interval is 10 m s^{-1}. The temperature field is superimposed also by the dashed contours with a contour interval of 10 K. In (b), the solid (negative) contours denote a "clockwise" ("counter-clockwise") circulation. The contour interval is nonuniform.

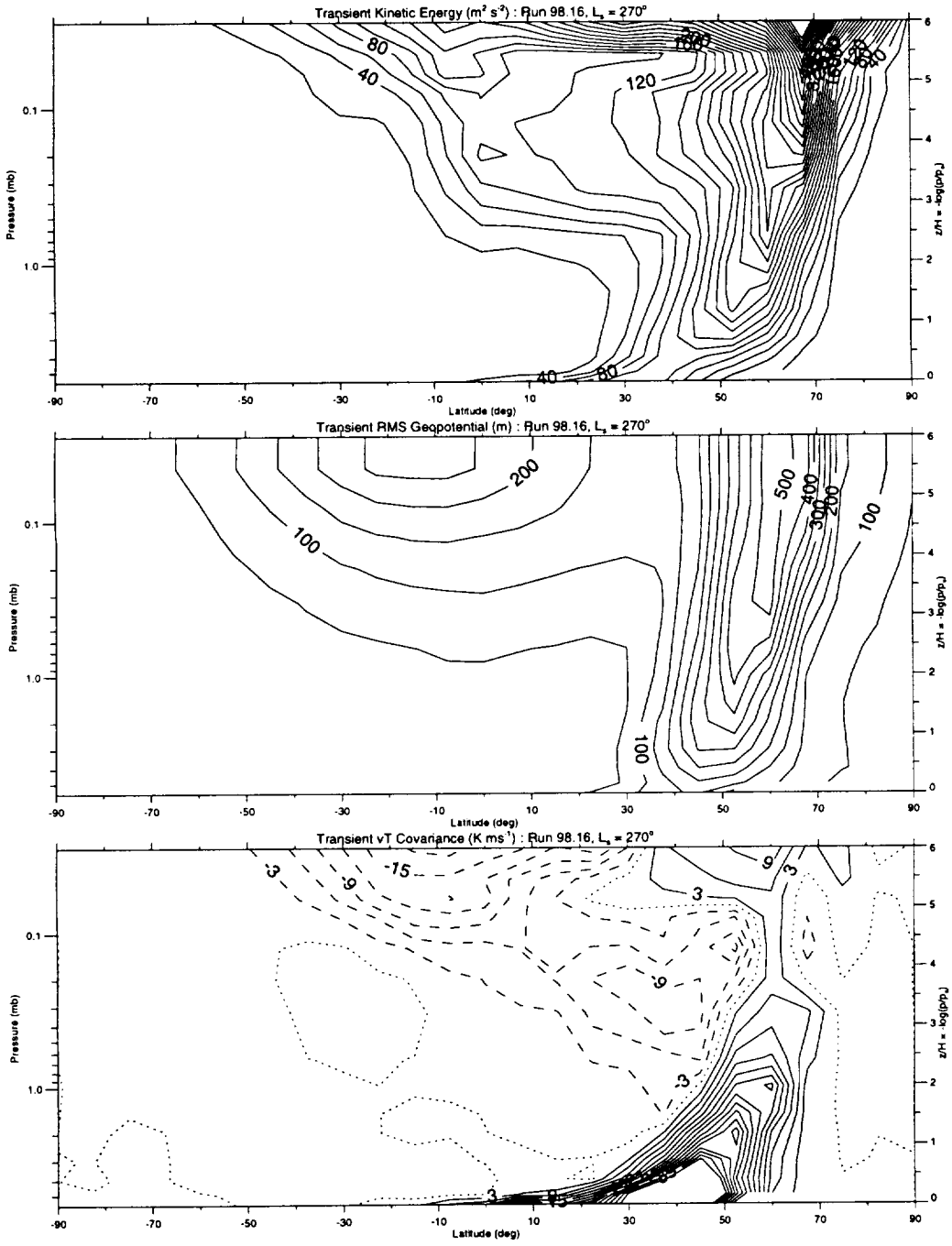

Figure 2: Transient-eddy statistics from a dynamical core simulation with the Mars General Circulation Model (with no surface topography) at 7.5 × 9.0° horizontal resolution and 16 vertical layers using the $L_s = 270°$, $\tau = 0$ radiative-equilibrium relaxation field with a relaxation time constant $\tau_{\text{radeq}} = 2$ days: (a) eddy kinetic energy ($m^2\ s^{-2}$); (b) eddy geopotential height (m); and (c) eddy horizontal heat flux, $[\overline{v'T'}]$ (m K s^{-1}). The contour interval is 20 $m^2\ s^{-2}$, 50 m, and 3 m K s^{-1}, in (a)-(c), respectively, and negative values in (c) are dashed.

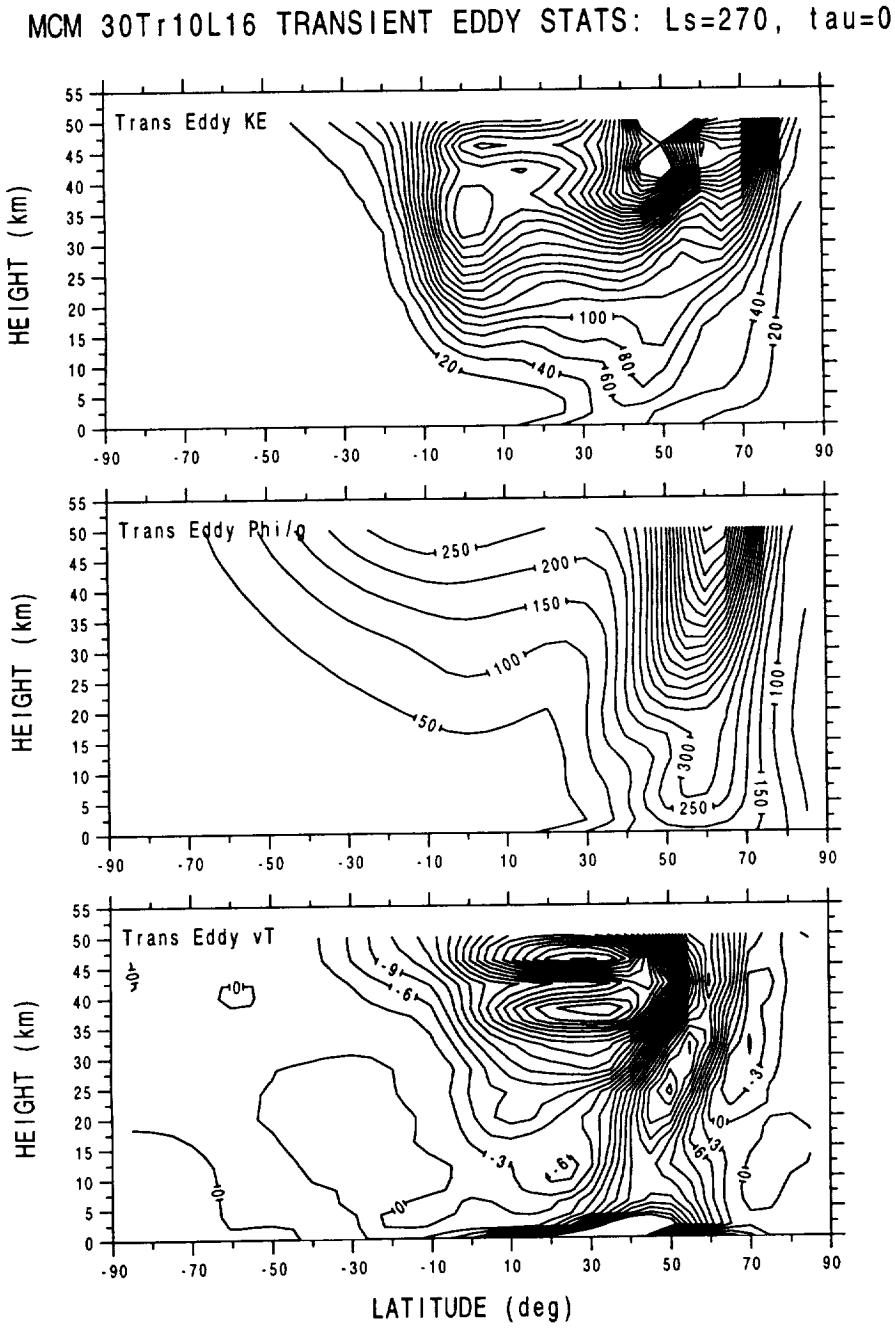

Figure 3: Transient-eddy statistics from a simulation with the Mars Climate Model (MCM) at a 30Tr10L16 truncation using the $L_s = 270°$, $\tau = 0$ radiative-equilibrium relaxation field with a relaxation time constant $\tau_{radeq} = 2$ days: (a) eddy kinetic energy ($m^2\ s^{-2}$); (b) eddy geopotential height (m); and (c) eddy horizontal heat flux, $[\overline{v'T'}]$ (m K s^{-1}). The contour interval is 20 $m^2\ s^{-2}$, 50 m, and 3 m K s^{-1}, in (a)-(c), respectively, and negative values in (c) are gray shaded.

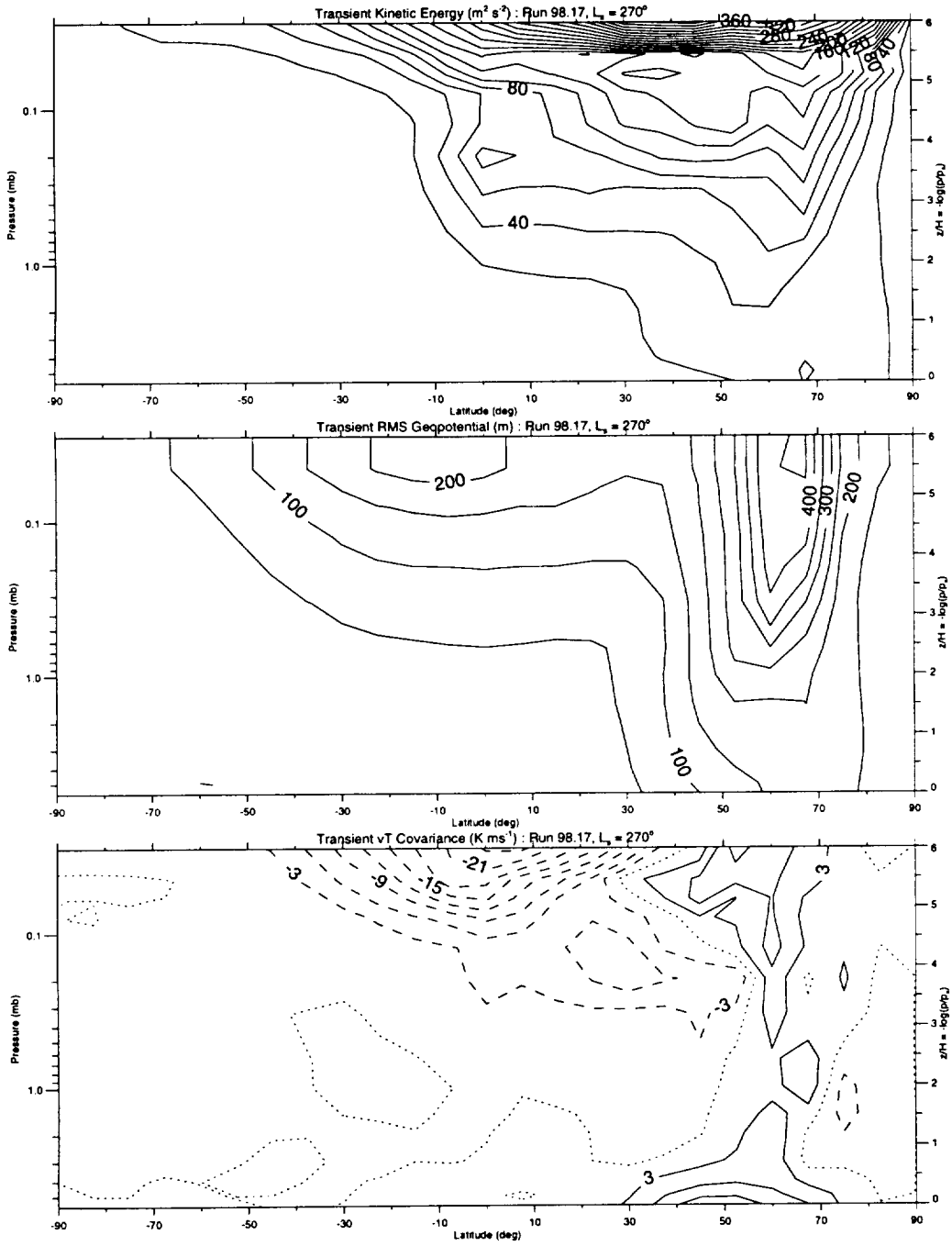

Figure 4: As in Figure 2 but for a simulation that includes spatially varying surface topography. The topography corresponds to the Smith and Zuber (1996) dataset.

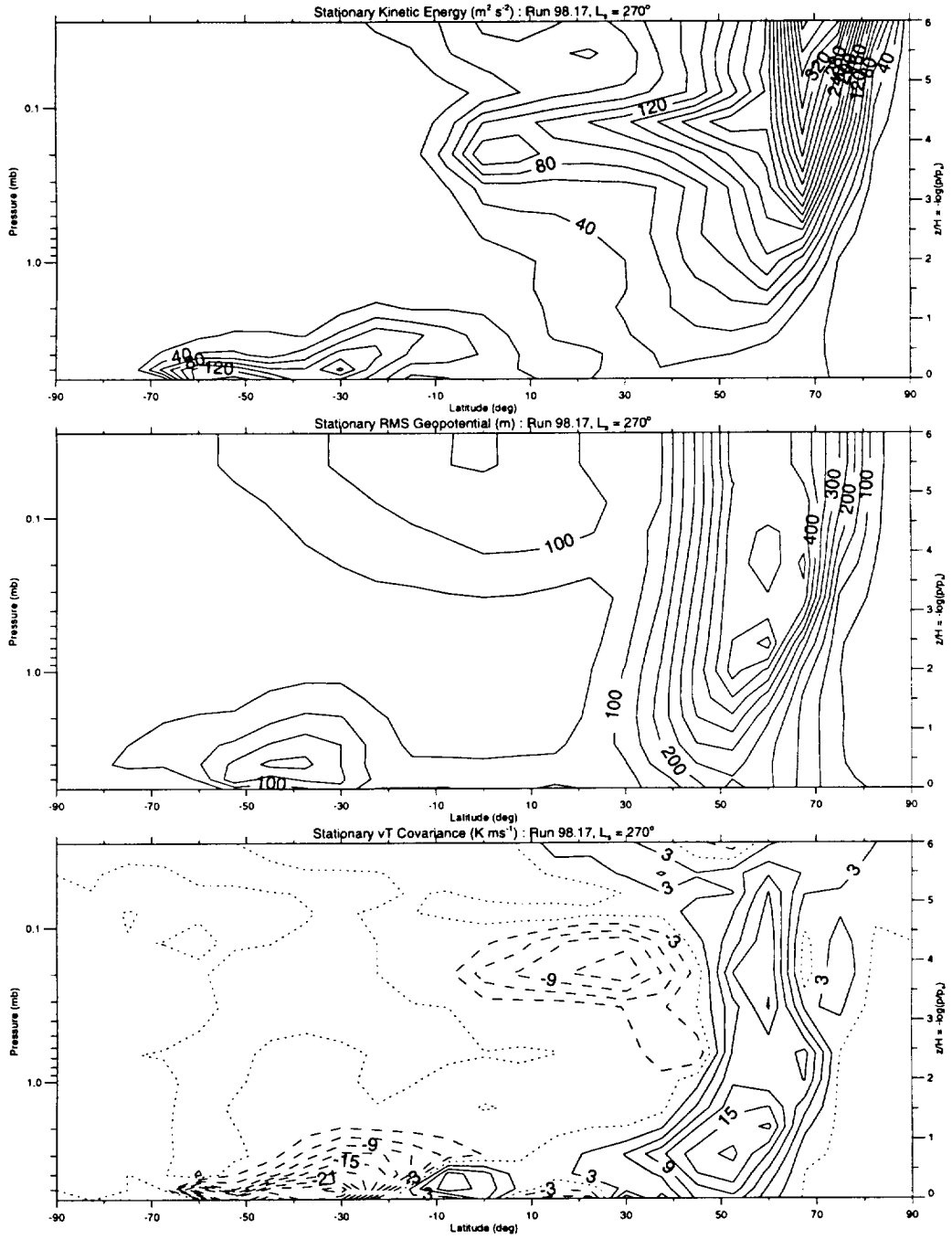

Figure 5: As in Figure 3 but for the zonal RMS stationary eddy fields.

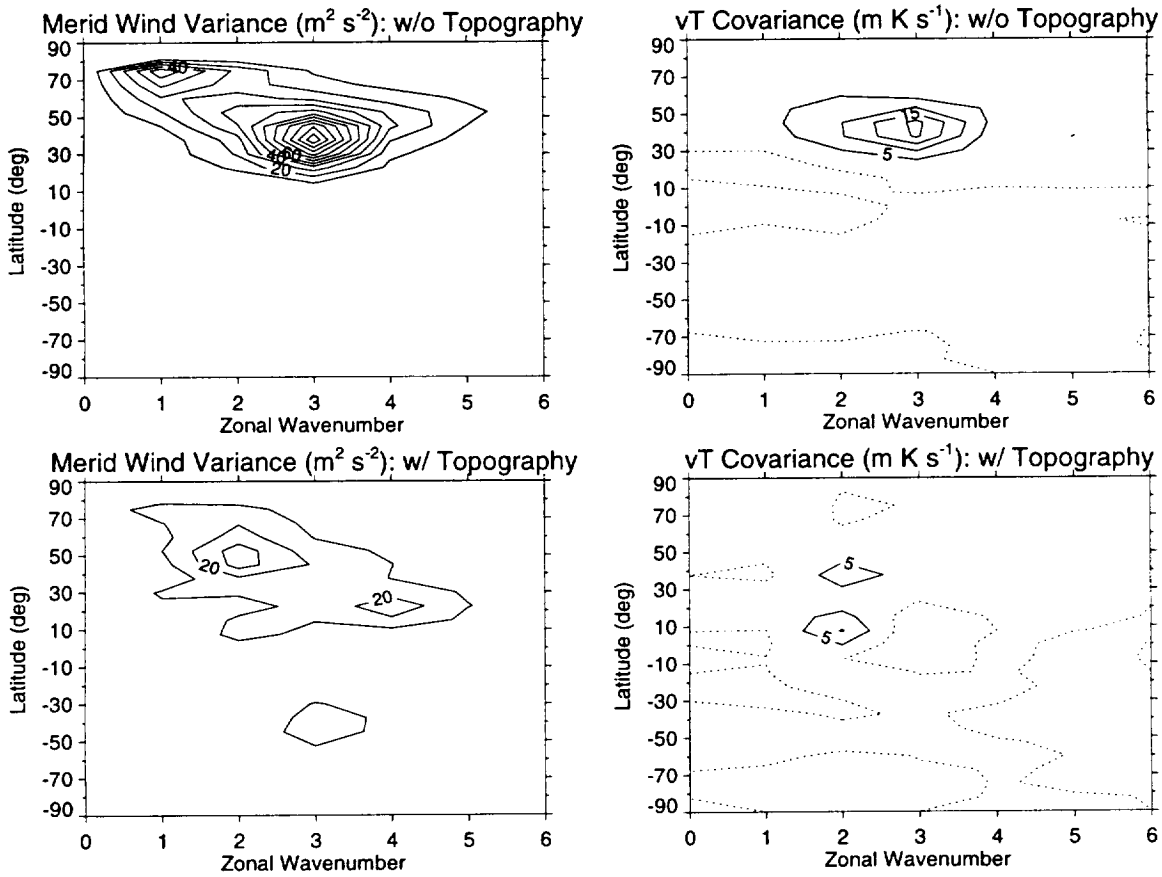

Figure 6: Zonal wavenumber spectra near the 3.0 mbar level of transient eddy (a) meridional wind variance ($m^2\ s^{-2}$) and (b) meridional wind and temperature covariance ($m\ K\ s^{-1}$) in the no topography simulation; (c) as in (a), and (d) as in (b) but in the full topography simulation. The topography corresponds to the Smith and Zuber (1996) dataset. The contour intervals are 10 ($m^2\ s^{-2}$) in (a) and (c), and 5 ($m\ K\ s^{-1}$) in (b) and (d), respectively. Negative values in (b) and (d) are dashed.

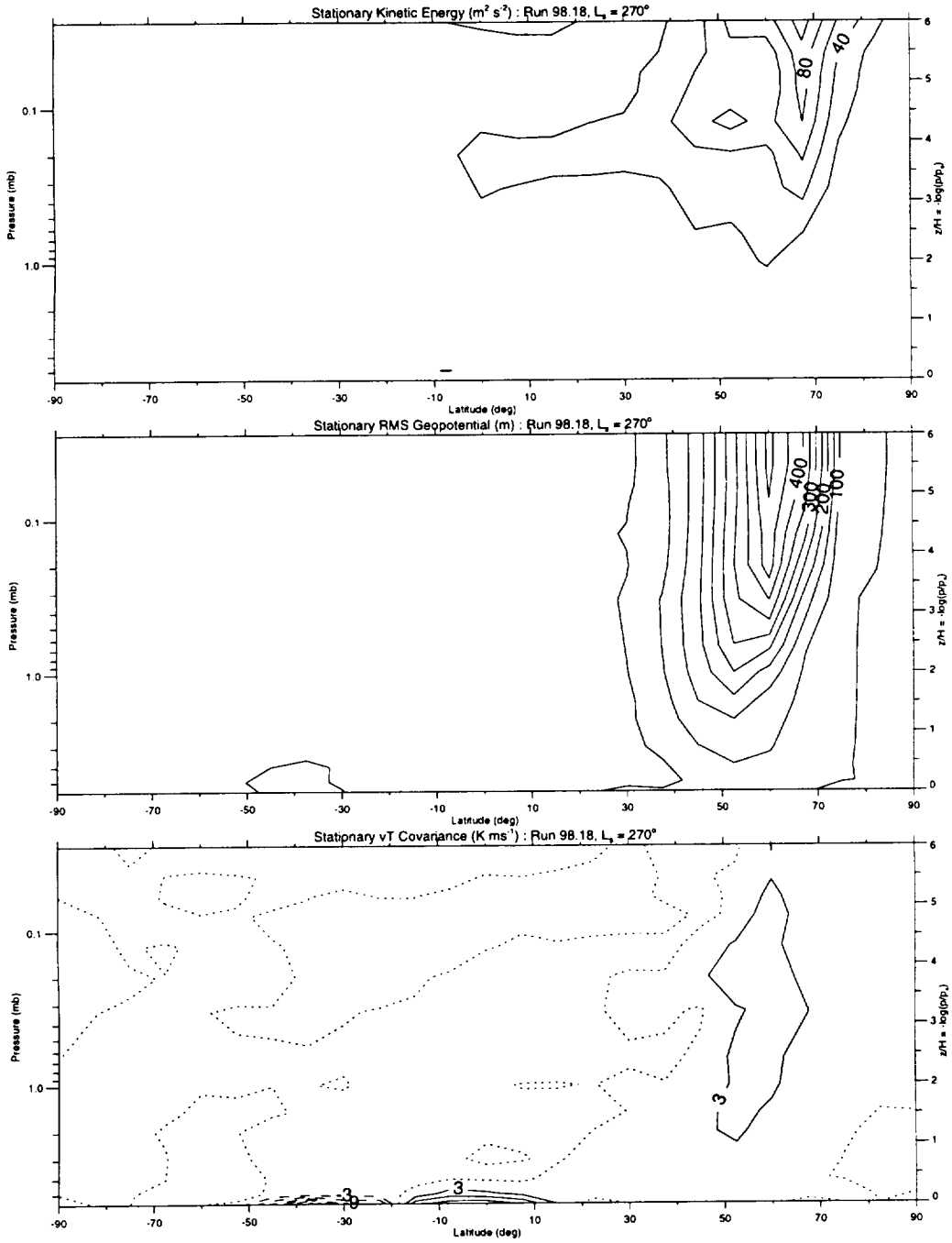

Figure 7: As in Figure 5 but for a dynamical core simulation with topography scaled by 0.2.

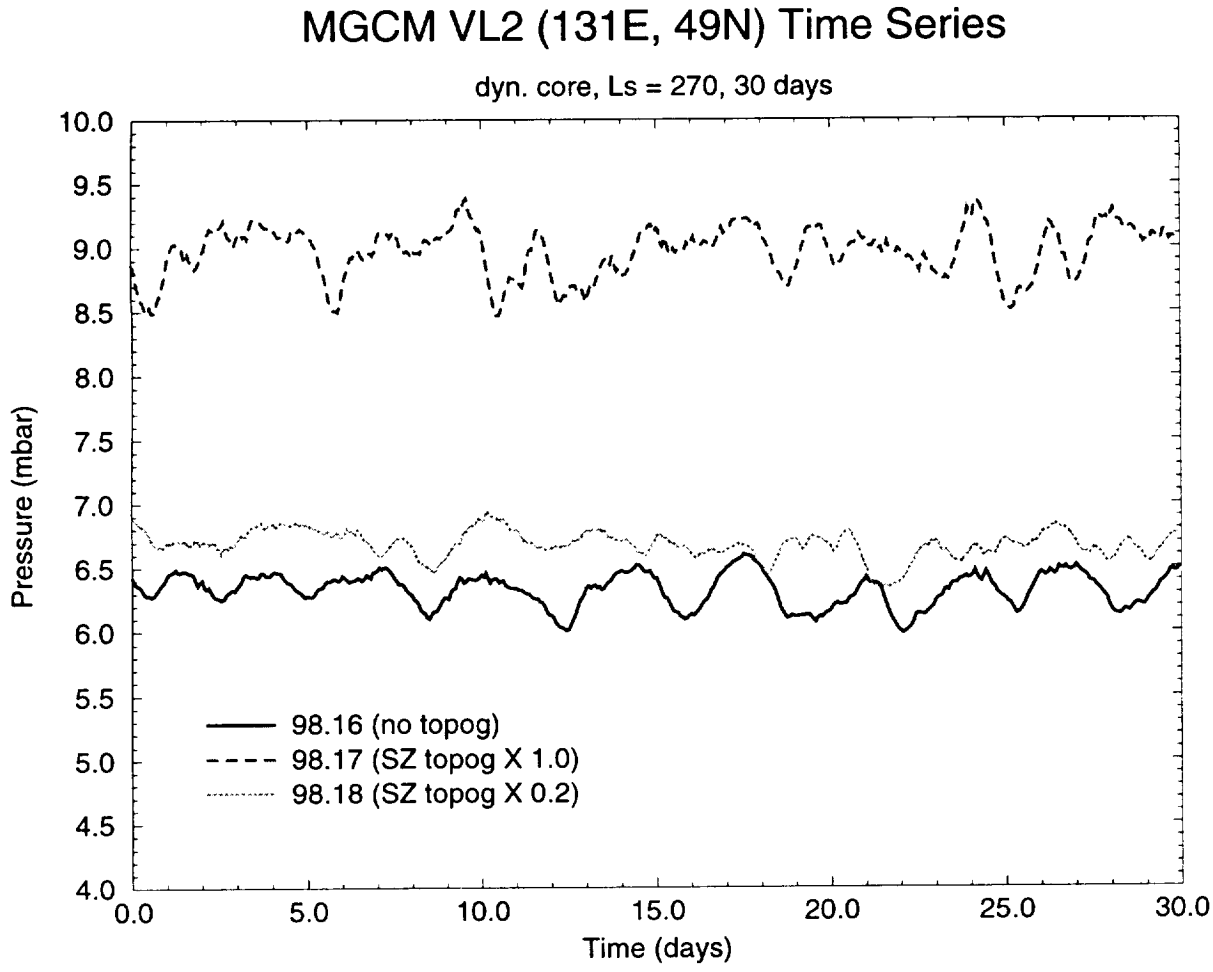

Figure 8: Time series of surface pressure at the grid point nearest the VL2 Lander site (131°E, 49°N) in the MGCM for three dynamical core simulations ($L_s = 270°$, $\tau = 0$, $\tau_{radeq} = 2$ days) with scaled topography. The topography corresponds to the Smith and Zuber (1996) dataset.